Acta Crystallographica Section A
Foundations of Crystallography
ISSN 0108-7673

Received 19 September 2001
Accepted 21 March 2002

Dedicated to Professor T. Janssen on the occasion of his 65th birthday

Morphological possibilities in general crystallography. Snow crystals

A. Janner

Institute for Theoretical Physics, University of Nijmegen, Toernooiveld, 6525 ED Nijmegen, The Netherlands. Correspondence e-mail: alo@sci.kun.nl

Morphological features of snow crystals are analyzed on the basis of concepts of a general crystallography, where point groups of infinite order are possible. The observations are first formulated in a set of rules, leading to a macroscopic growth lattice and to continuous growth boundaries. Both are brought in connection with two-dimensional integral invertible transformations. Families of boundaries are considered, labeled by a set of indices restricted by selection rules and generalizing the law of rational indices. These properties are indicated graphically on a sample of 12 natural snow crystals. Their geometric and arithmetic properties are summarized in a table.

1. Introduction

General crystallography is characterized by the possibility of point groups of infinite order isomorphic to groups of integral matrices (Janner, 2001*b*). These groups have never been considered in crystallography because of the implicit assumption that the symmetry group of a Euclidean object (the crystal) is necessarily Euclidean. This need not be the case. So, for example, the lattice of a hexagonal close packing is invariant with respect to a point group of infinite order implying the ratio $c/a = (8/3)^{1/2}$. This same point group allows one to characterize in terms of symmetry elements the octahedral and the tetrahedral sites of this close packing, which, otherwise, require the specification of a parameter whose value is not fixed by the corresponding Wyckoff positions.

This means that there are Euclidean structural properties only expressible in terms of non-Euclidean symmetries. It is, therefore, not surprising that these infinite point groups occur in nature more often than one would think. Their relevance, however, is not generally recognized, because the implications have been worked out only in very few special cases.

One finds one of these few cases in the morphology of snow crystals. On the basis of the infinite point group of an extended space group leaving the structure of ice invariant, characteristic hexagrammal scaling properties of snow flakes could be recognized and interpreted (Janner, 1997). Another, completely different, case where a similar point group plays a role is given by hexagonal nucleic acids in helical conformation (Janner, 2001*a*). Again, the corresponding hexagonal molecular forms reveal hexagrammal scaling properties. In these cases, the molecular form is a polyhedron that encloses a periodic unit of the secondary structure having, of course, a hexagonal point-group symmetry. Moreover, atomic positions of the molecular asymmetric unit of this Euclidean point group could be related by elements of the larger point group. Actually, the investigation of biomacromolecules started from globular proteins with a given axial point-group symmetry, where similar scaling properties have been recognized (Janner, 1996). All this simply means that systems with a given Euclidean point-group symmetry can have hidden a much larger symmetry group.

The aim of this work is to point out, at a geometric level, morphological properties of snow crystals, secondary structure of nucleic acids and quaternary structure of proteins, which are compatible with a crystallographic point group of infinite order, as it is conceptually possible in general crystallography.

This first paper deals with snow crystals, developing further a previous morphological investigation (Janner, 1997), here denoted as *Nive*. Columnar snow crystals are disregarded and the description of the planar ones is two dimensional. In §2, the existence of a macroscopic hexagonal lattice Λ is pointed out that underlies the morphology of snow flakes. Moreover, different types of boundaries are observed, which connect points of this lattice. In addition to the familiar flat boundary, circular and hyperbolic ones also occur. General properties of these boundaries are formulated as rules, deduced from the morphology of a number of natural snow crystals. In §3, these boundaries are analyzed in terms of point-group transformations leaving the lattice Λ invariant, but not necessarily the underlying microscopic structure of ice. Indeed, these boundaries can be characterized by automorphisms of the lattice Λ, implying crystallographic restrictions on the continuous linear transformations generating the observed boundaries, with beginning and end at points of the lattice Λ. This leads, in §4, to consideration of families of boundaries sharing the same end points and to characterize morphological features of snow crystals in terms of sets of integers (*indices*), restricting by selection rules the possible (more stable) growth boundaries. In fact, this formulation corresponds to an extension of the law of rational indices. In §5, the geometric

and arithmetic properties of the growth boundaries observed (and drawn) in the snow crystals selected for deriving the rules of §2 are summarized in a tabular overview. Finally, mathematical details on the derivation of the expressions in §3 can be found in Appendix *A*.

As pointed out in the conclusion, this analysis does not exhaust the rich complexity of snow flakes. In particular, only the patterns of possible growth boundaries are considered here among those characterized in *Nive*. The validity of hexagrammal scaling is verified in the new samples as well.

2. Observations

Before dealing with the mathematical aspects of a crystal morphology based on the existence of an infinite crystallographic point group, new features are pointed out in terms of phenomenological rules deduced from a number of snow crystals. The sample (BW 1) that represents the simplest nontrivial case has been redrawn from an article published in *Bild der Wissenschaft* (Olovsson, 1985). All other snow flakes have been reproduced (by courtesy of Dover) from the book of

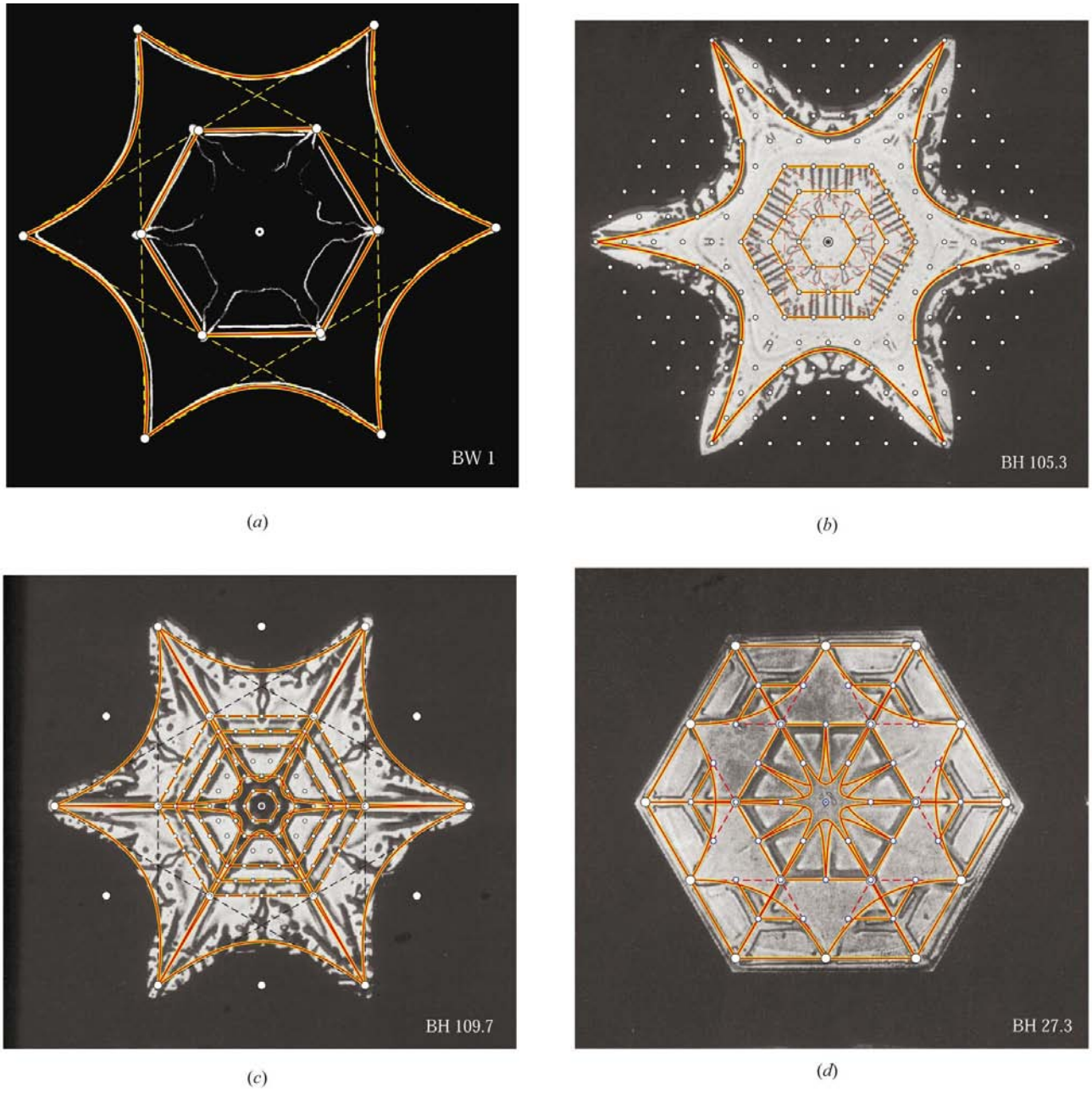

Figure 1
Snow crystals with hexagonal flat boundaries combined with hyperbolic ones through points of the growth lattice. The lattice points are indicated by empty circles with a size reflecting the corresponding lattice–sublattice relation. The sample BW 1 has been redrawn from Olovssson (1985). The other snow flakes have been taken from Bentley & Humphreys (1931) *Snow Crystals* (courtesy Dover). (*a*) BW 1, (*b*) BH 105.3, (*c*) BH 109.7 and (*d*) BH 27.3.

Bentley & Humphreys (1931), and are labeled accordingly (with BH followed by the page and the position numbers, as already done in *Nive*). The attention is focused on geometric properties of sets of observed boundary lines (see Figs. 1 to 5).

Rule 1. The same type of shape, which occurs as external boundary of a crystal growth form, is also observed as an internal pattern. Both are, therefore, denoted as *growth boundaries*, independently of whether internal or external.

The regular hexagon is very frequent as a growth form or as an internal pattern [see *e.g*. BH 27.3 of Fig. 1(*d*), BH 39.8 of Fig. 2(*b*), and many other cases]. The hexagrammal form of BH 145.7 can be seen as internal pattern in BH 141.11 (not reproduced here, see Fig. 5 of *Nive*). Various hyperbolic hexagons occur as external or internal boundaries in BW 1, BH 105.3, BH 109.7, BH 27.3 and BH 39.8. The same circular shape of BH 63.12 appears as internal in BH 33.5 and in BH 145.12 as external and as internal boundary in a scaling ratio 1 to 12.

Rule 2. There are three types of growth boundaries, characterized by their curvature: flat ones with curvature zero, hyperbolic ones with negative curvature and elliptic ones (circular in particular) with positive curvature.

Flat faces (here given by straight segments) are the natural thermodynamic equilibrium growth boundaries in crystals. In snow, they normally appear as growth forms in facet-like crystals and as skeletons in the dendritic flakes. I became aware of the morphological importance of hyperbolic boundaries while looking at the cover picture of an article by Olovsson published in *Bild der Wissenschaft* (Olovsson, 1985). There, a (nearly) regular hyperbolic hexagon appears together, and in a scaling relation 2 to 1, with a Euclidean regular hexagon. Moreover, both are connected by an underlying star hexagon (see BW 1 in Fig. 1*a*). Many more examples followed by looking at the book of Bentley & Humphreys (1931) (see BH 105.3, BH 109.7, BH 27.3, BH 39.8 and even in the triangular form of BH 205.10, not reproduced here). It was then natural to search for snow crystals having boundaries with positive curvature. A number of cases could easily be identified involving circles (see BH 33.5, BH 145.12, BH 63.12 and the central part of BH 39.8). The elliptic (non-circular) case seems to be much rarer: there is one example in BH 145.7. It is evident that these various possibilities arise from a combination of symmetry (the sixfold one, in particular) with conditions of growth, which differ from flake to flake, or for a given crystal, when changes occur in the growth conditions. This remark should help to bridge the gap between the geometry of growth boundaries with the physics of crystal growth.

Rule 3. Scaling relations among growth boundaries of a given crystal can be expressed by means of a macroscopic *growth lattice*. If several such lattices occur, they share the same center and are in a lattice–sublattice relation, the smaller elementary cell being observed towards the center.

This macroscopic lattice cannot be explained on the basis of the lattice periodicity of the microscopic structure only. A possible explanation involves two mechanisms, which are not mutually exclusive. The first one assumes an intermittent growth, periodic in time, giving rise to a macroscopic peri-

(*a*)

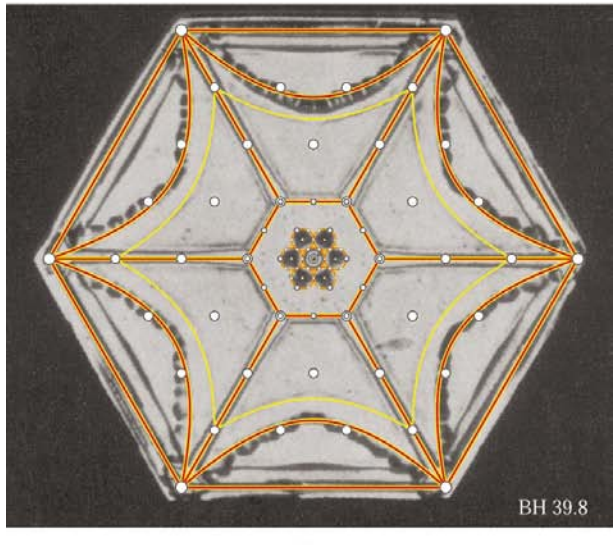

(*b*)

Figure 2
In these snow crystals, in addition to the parabolic (flat) boundaries and to the hyperbolic ones, one observes elliptic boundaries in (*a*) BH 145.7 and circular ones in (*b*) BH 39.8 (courtesy Dover). The growth lattices are indicated as in Fig. 1.

odicity in space. The second one is based on the existence of the infinite crystallographic point group leaving the ice structure invariant, as shown in *Nive*, and requires two singularities. A first singularity, represented by the seed at the beginning of the growth process, fixes the distinguished center invariant with respect to the point group (the center of the snow flake). A second singularity (possibly also a seed) gives rise to a fairly large number of point-group-equivalent positions (say for other seeds), infinite in principle but not in practice, around the center. Apparently to allow growth, this second singularity has to be on one of the hexagonal mirror planes, equivalent either to m_x or to m_y. Therefore, this singularity can be taken to be at [1 0] position of a lattice either in the same orientation of the microscopic lattice of the symmetry translations, or turned by $\pi/2$ with respect to it. This second explanation, adopted in *Nive*, allows the hexagrammal scaling properties and other morphological features to be interpreted. The existence of growth boundaries associated with a concentration of impurities suggests that both growth mechanisms are at work. This would also explain the increasing of the elementary cell in a lattice–sublattice relation. A lattice point reached at a given stage of the growth could represent a new singularity generating a larger lattice by the point-group mechanism. Alternatively, the time scale of

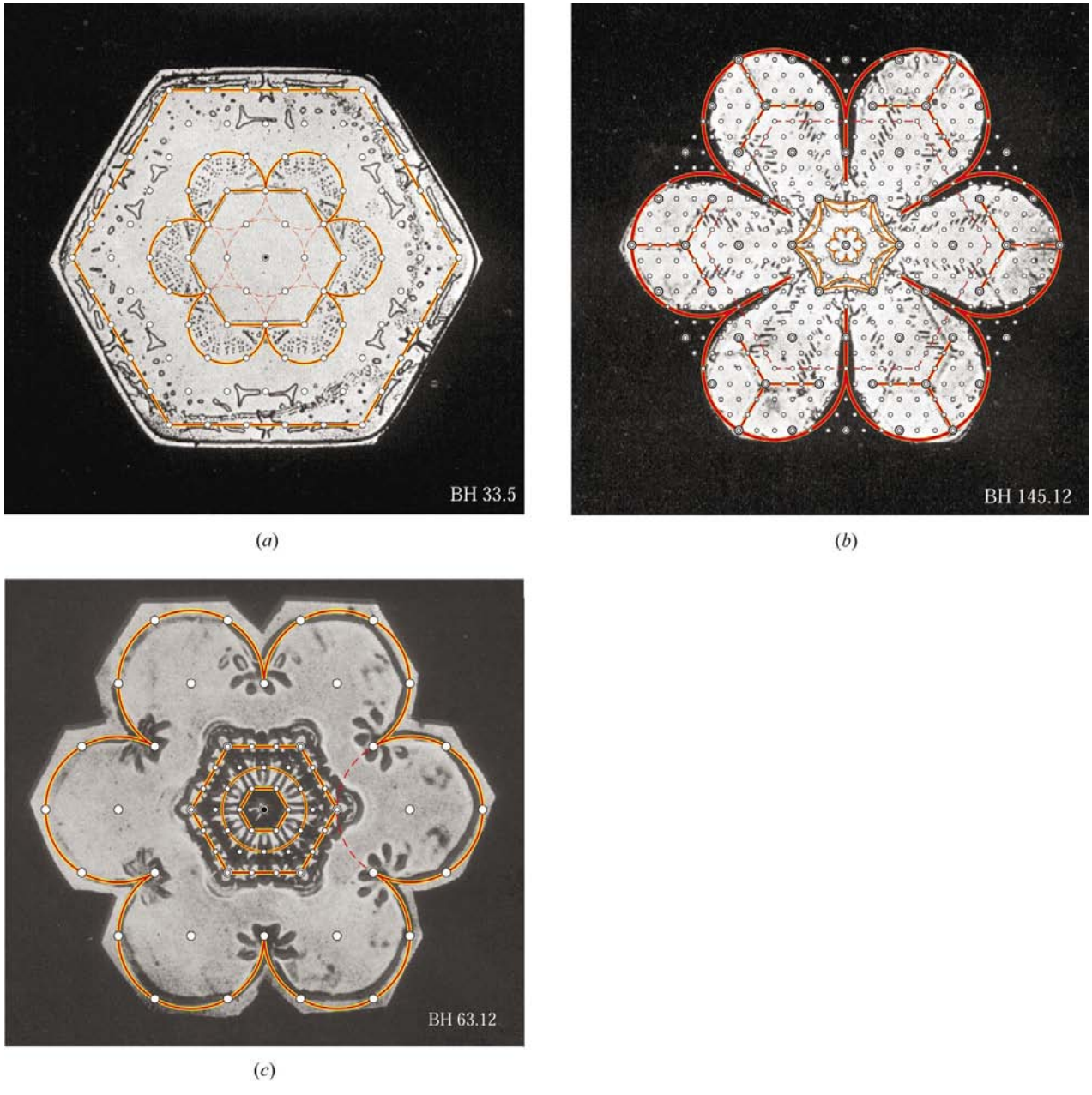

Figure 3
Snow crystals with circular boundaries centered at points of the growth lattice and with a radius given by a lattice vector: (*a*) BH 33.5, (*b*) BH 145.12 and (*c*) BH 63.12 (courtesy Dover).

the growth periodicity can be assumed to be proportional to the size of the crystal already reached. One has, however, to distinguish between two types of impurities: those giving rise to seeds in the crystallization process and appearing as singularities at points of the growth lattice, and all the other impurities, which simply accumulate at the growth boundaries (by the same mechanism as in a zone-melting experiment). At present, all these considerations are conjectures only, even if compatible with the empirical evidence.

In the examples of Figs. 1 to 5, the various growth lattices are indicated by empty circles with a size suggesting the lattice–sublattice relation. So for example in BH 39.8, the central circular growth lines are associated with a first lattice. A second lattice arises at the corresponding extremal points and leads to a regular hexagon, with vertices generating a third lattice with hyperbolic boundaries, and a final one defined by the largest hexagon. The corresponding lattice–sublattice relations are here in the ratios 1:3:6:18:24.

Rule 4. Morphological relevant growth boundaries have piece-wise beginning and end at points of the growth lattice. These lines are generated by linear transformations restricted by crystallographic conditions implying that beginning and end points are related by an automorphism of the growth lattice and, accordingly, have origin at a lattice point (normally the center).

Lattice automorphisms expressed with respect to a lattice basis are invertible integral matrices, two-dimensional in our case. Depending on the value of the trace n, they are *hyperbolic* (for $|n| > 2$), *parabolic* (for $|n| = 2$, if not the identity or the total inversion) and *elliptic* (for $|n| < 2$), because the corresponding automorphisms transform lattice points along hyperbolas, straight lines or ellipses (and circles), respectively. All the lines added to the snow flakes of Figs. 1 to 5 as an idealization of the growth boundaries have been drawn according to Rule 4. This rule is fairly restrictive. Indeed, the only allowed rotation angles are $\varphi_n = \arccos(n/2)$ in the elliptic case and $\chi_n = \cosh^{-1}(n/2)$ in the hyperbolic case.

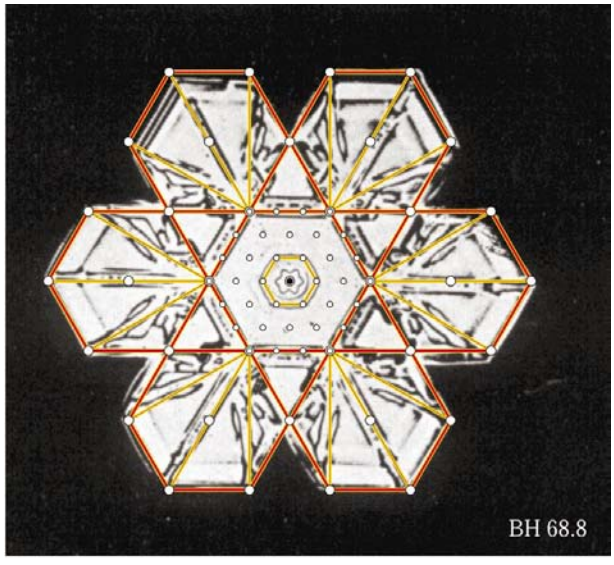

(*a*)

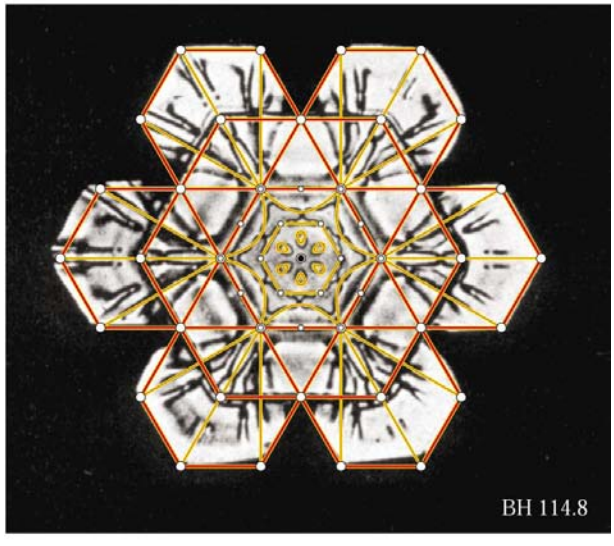

(*b*)

Figure 4
Facet-like snow flakes with a morphology based on regular hexagons with centers and vertices at points of the growth lattice. In the central region, one observes hyperbolic and elliptic boundaries based on a finer growth lattice. The branching points can be related to the occurrence of degenerate hyperbolic boundaries. (*a*) BH 68.8 and (*b*) BH 114.8 (courtesy Dover).

Figure 5
The dendritic snow flakes are based on degenerate hyperbolic boundaries with branching sites at points of the growth lattice and giving rise to a hexagrammal structure. In the central region of the sample BH 167.8, one finds regular hexagons scaled according to a finer growth lattice. One even sees hyperbolic boundaries turned by 30° with respect to the lattice orientation, in the same way as observed in BH 27.3 of Fig. 1(*d*).

Additional restrictions apply, which need a more mathematical approach to be discussed.

These lattice automorphisms, in general, do not leave the microscopic structure of ice invariant, but the deviations are macroscopically irrelevant, in the same way as in the morphology of a crystal non-primitive translations are of secondary importance only. Indeed, applying an automorphism of the growth lattice to an arbitrary atomic position, one gets a deviation (with respect to a space-group equivalent position) that is always microscopically small, even if an additional rotation by $\pi/2$ is required when the growth lattice does not have the same orientation as the lattice of symmetry translations.

3. Automorphisms of the growth lattice

In this section, a geometric characterization of growth boundaries is given in terms of automorphisms of the hexagonal growth lattice Λ. The transformations considered are expressed in the lattice basis $a = \{a_1, a_2\}$:

$$a_1 = a_0(1, 0), \quad a_2 = a_0(-1/2, 3^{1/2}/2), \tag{1}$$

with components given in the orthonormal basis $e = \{e_1, e_2\}$ and a_0 the macroscopic cell parameter. This means that Λ is chosen in the x orientation. The lattice of symmetry translations has either the same or the alternative y orientation.

Rule 4 implies that the growth boundaries are piece-wise generated by elements of the connected component of the unity of the general linear group $GL(2, \mathbb{R})$ of the real invertible two-dimensional matrices. In this set, there are two distinguished subsets of elements: the ones that leave the beginning point invariant, and the lattice automorphisms that transform the beginning to the end point. Both belong to the subgroup $GL(2, \mathbb{Z})$ of the invertible integral matrices of the same dimension. As usual, $\mathbb{R}$ denotes the set of real numbers and $\mathbb{Z}$ the rational integers. Attention will first be paid to the lattice automorphisms because they restrict the admitted linear transformations and, accordingly, the growth boundaries satisfying crystallographic conditions.

In the basis a, one has:

$$A(a) = \begin{pmatrix} \alpha & \beta \\ \gamma & \delta \end{pmatrix} \in GL(2, \mathbb{Z}),$$
$$\det A = 1 \text{ and } \alpha + \delta = n > -2. \tag{2}$$

The restrictions on the determinant and on the trace are required because the corresponding linear transformation has to belong to the connected component of the identity for ensuring the continuity observed in the boundaries. It is convenient to express the geometric properties of A as a function of the three integers n, β and δ fulfilling the conditions:

$$\beta \neq 0, \quad (\beta, \delta) = 1, \quad \gamma = [(n - \delta)\delta - 1]/\beta \in \mathbb{Z}. \tag{3}$$

Accordingly, the lattice point [0 1] is transformed by A into $[\beta\, \delta]$. The case $\beta = 0$ can be treated in the same way after transposition because, for A not the identity or the total inversion, $\beta = 0$ implies $\gamma \neq 0$. Morphologically, the parabolic case is the most important, followed by the hyperbolic one and then by the elliptic case, which mainly appears as the circular one. These three cases will now be discussed.

3.1. Flat growth boundaries

A flat boundary connecting two points of the growth lattice Λ belongs to a lattice line. Such a line is perpendicular to a reciprocal-lattice vector $k = (k_1\, k_2) \in \Lambda^*$, whose integral components (here expressed in the dual lattice basis $a^* = \{a_1^*, a_2^*\}$) are the indices of the line. In three dimensions, and without growth lattice, this is simply the *law of rational indices* for flat crystal facets. In the case of a growth lattice, however, there is a distinguished center (see Rule 3) and straight lines passing, or not, through the center have a different character. Those through the center represent in fact degenerate hyperbolic transformations and will be discussed in the next subsection, whereas the other lines are obtained from parabolic transformations.

In two dimensions, a parabolic lattice automorphism P has trace $n = 2$. It is convenient to express the other two matrix elements β and δ in terms of a lattice vector $v = [v_1\, v_2] \in \Lambda$. With $\beta = v_1$, $\delta = 1 + v_2$, one has:

$$P_v(a) = \begin{pmatrix} 1 - v_2 & v_1 \\ -v_2^2/v_1 & 1 + v_2 \end{pmatrix}, \quad v_1 \neq 0, \tag{4}$$

such that v_1 and $1 + v_2$ are relatively prime integers and v_1 divides v_2^2. As already mentioned, the case $v_1 = 0$, which implies $v_2 \neq 0$, can be treated in a similar way. Instead of (4), one then has:

$$P'_v(a) = \begin{pmatrix} 1 + v_1 & -v_1^2/v_2 \\ v_2 & 1 - v_1 \end{pmatrix} = \begin{pmatrix} 1 & 0 \\ v_2 & 1 \end{pmatrix}, \quad v_2 \neq 0. \tag{5}$$

A lattice point $m = [m_1\, m_2]$ (after identification of lattice points with lattice vectors) is then transformed by P_v into another lattice point m' along the invariant direction of v. Indeed,

$$P_v(a)m = m + (1/v_1)(v_1 m_2 - v_2 m_1)\, v = m' \in \Lambda, \tag{6}$$

and in particular

$$P_v(a)\, v = v, \tag{7}$$

so that the line indices $(k_1\, k_2)$ are related to the invariant vector $v = [v_1\, v_2]$ by

$$[v_1\, v_2] \cdot (k_1\, k_2) = k_1 v_1 + k_2 v_2 = 0 \tag{8}$$

as k is perpendicular to v. One can assume that k_1 and k_2 are relatively prime integers, and one can take $v_1 = v_0\, k_2$ and $v_2 = -v_0\, k_1$, with v_0 the greatest common divisor of v_1 and v_2, which is indicated as $v_0 = (v_1, v_2)$. The corresponding set of continuous parabolic transformations, generating a flat growth boundary beginning at the lattice point m and ending at m', when expressed in terms of the line indices $(k_1\, k_2)$, is given by:

$$P_\tau(a) = \begin{pmatrix} 1 + \tau k_1 & \tau k_2 \\ -\tau k_1^2/k_2 & 1 - \tau k_1 \end{pmatrix}, \quad k_2 \neq 0, \tag{9}$$

with $0 \leq \tau \leq v_0$. The case $k_2 = 0$, and thus $k_1 \neq 0$, follows after a transposition and one has correspondingly $k_1 = v_2/v_0$, $k_2 = -v_1/v_0$.

Even if all line indices can occur, it does not mean that any pair of lattice points lying on a given lattice line is a possible begin–end pair of a growth boundary, because they have to be related by a parabolic automorphism of the growth lattice. Therefore, the crystallographic conditions imposed on flat boundaries are more severe for crystal forms with growth lattice than without, as in the normal crystal morphology.

3.2. Hyperbolic growth boundaries

Hyperbolic growth boundaries have beginning and end points connected by an automorphism L_n, with trace $n > 2$, transforming the lattice points along hyperbolic lines. In a lattice basis, the corresponding matrix has integral entries and there is an orthonormal basis e', rotated with respect to the x and y axes, allowing L_n to be expressed as an affine hyperbolic rotation. In particular, one has [recall the conditions indicated in (3)]:

$$L_n(a) = \begin{pmatrix} n-\delta & \beta \\ [(n-\delta)\delta - 1]/\beta & \delta y \end{pmatrix}, \tag{10}$$

$$L_n(e') = \begin{pmatrix} \cosh\chi_n & \sigma_n \sinh\chi_n \\ \sinh\chi_n/\sigma_n & \cosh\chi_n \end{pmatrix}, \tag{11}$$

with corresponding bases a and e':

$$\begin{aligned} a_1 &= a_0\, e_1 & e'_1 &= e_1 \cos\phi_n + e_2 \sin\phi_n \\ a_2 &= a_0[-\tfrac{1}{2}e_1 + (3^{1/2}/2)e_2] & e'_2 &= -e_1 \sin\phi_n + e_2 \cos\phi_n. \end{aligned} \tag{12}$$

The geometry of L_n follows from the real parameters χ_n (the hyperbolic rotation angle), σ_n (the affine deformation factor), ϕ_n (the rotation angle of the orthonormal system e', which also gives the angle formed by the symmetry axis of the hyperbola with the x axis) and ω_n (the angle between the asymptotes of the hyperbola) expressed in terms of the integral parameters n, β, δ of the automorph of the growth lattice. Details of the computation are postponed to Appendix A. The general expressions are:

$$\chi_n = \cosh^{-1}(n/2) \tag{13}$$

$$\sigma_n = \frac{2}{3^{1/2}} \frac{z_1 + r_{12}}{\beta(n^2-4)^{1/2}} \tag{14}$$

$$\phi_n = \arctan[z_2/(z_3 + r_{12})] \tag{15}$$

$$\omega_n = \arccos(z_1/r_{12}), \tag{16}$$

where (up to a sign of the square roots)

$$\begin{aligned} r_{12} &= [z_0 n^2 + (\beta - 2\delta)(z_0+1)n + z_0^2 + 2z_0 - 3\beta^2 + 1]^{1/2} \\ z_0 &= \beta^2 - \beta\delta + \delta^2 \\ z_1 &= (\beta/2 - \delta)n + z_0 + 1 \\ z_2 &= (3^{1/2}/2)[(-\beta + \delta)n + (2\beta - \delta)\delta - 1] \\ z_3 &= \tfrac{1}{2}[(\beta + \delta)n - 3\delta^2 + 2z_0 - 1]. \end{aligned} \tag{17}$$

The growth boundaries with beginning and end points related by the automorphism L_n are generated by continuous σ_n-deformed hyperbolic rotations, which, in the rotated orthonormal basis e', take the simple form

$$L_\chi(e') = \begin{pmatrix} \cosh\chi & \sigma_n \sinh\chi \\ \sinh\chi/\sigma_n & \cosh\chi \end{pmatrix}, \quad 0 \leq \chi \leq \cosh^{-1}\frac{n}{2}. \tag{18}$$

The degenerate case of a hyperbola reduced to straight lines is obtained in the limit $n \to \infty$. If one keeps β and δ finite, one gets:

$$\cos\omega_\infty = \frac{\beta - 2\delta}{2(\beta^2 - \beta\delta + \delta^2)^{1/2}} \tag{19}$$

$$\tan\phi_\infty = \frac{3^{1/2}(-\beta + \delta)}{\beta + \delta + 2(\beta^2 - \beta\delta + \delta^2)^{1/2}}. \tag{20}$$

The corresponding growth boundary is along the two straight lines that intersect at the center at an angle ω_∞ and have a bisecting line with slope given by ϕ_∞. It is the flat boundary case mentioned in §3.1, not due to a parabolic transformation.

3.3. The elliptic and circular growth boundaries

Lattice automorphs R_n of finite order 3, 4 and 6, with corresponding trace value $n = -1, 0, 1$, generate elliptic (and circular) growth boundaries. Their geometric characterization, given by essentially the same formulas as in the hyperbolic case, can now be described as an affine deformed circular rotation:

$$R_n(e') = \begin{pmatrix} \cos\varphi_n & -\rho_n \sin\varphi_n \\ \sin\varphi_n/\rho_n & \cos\varphi_n \end{pmatrix} \tag{21}$$

with

$$\varphi_n = \arccos(n/2), \tag{22}$$

$$\rho_n = \frac{2}{3^{1/2}} \frac{z_1 + r_{12}}{\beta(4-n^2)^{1/2}}, \tag{23}$$

$$\phi_n = \arctan\frac{z_2}{z_3 + r_{12}} \tag{24}$$

and r_{12}, z_0, z_1, z_2 and z_3 are the same expressions as in the hyperbolic case.

The elliptical growth boundaries are now generated by the ρ_n-deformed circular rotation:

$$R_\varphi(e') = \begin{pmatrix} \cos\varphi & -\rho_n \sin\varphi \\ \sin\varphi/\rho_n & \cos\varphi \end{pmatrix}, \quad 0 \leq \varphi \leq \arccos(n/2). \tag{25}$$

The circular boundaries follow for the special case $\rho_n^2 = 1$, which is equivalent to the condition $r_{12} = 0$, as derived in Appendix A. The symmetry axes of the ellipse are again along the orthonormal basis vectors e'_1 and e'_2 and the ratio between the two principal axes is given by ρ_n^2. For a hexagonal growth lattice, as assumed in this work, circular boundaries only occur for $n = \pm 1$, *i.e.* for a threefold or a sixfold rotation. The converse is not true because not all automorphs with $n = \pm 1$ are circular rotations.

4. Indexing growth boundaries

Indexing is a characterization of a geometric object, like a Bragg diffraction spot or a crystal lattice plane, by a set of rational integers (the *indices*). One knows how to label flat facets of crystal forms by rational indices. The growth boundaries discussed so far generalize these forms. The problem is to find a simple characterization in terms of a suitable set of integers (the new indices of the face), for the hyperbolic, the parabolic and the elliptic boundaries as well. The solution presented follows from mathematical and from physical considerations.

From a physical point of view, points of the growth lattice act as pinning centers by the formation of moving boundaries during the growth process. As flat (parabolic) boundaries correspond to the normal flat-facet case, it is natural to start from these and to consider hyperbolic and elliptic boundaries as a deformation of parabolic boundaries sharing the same beginning and end lattice points. From a mathematical point of view, such a transformation corresponds to a homotopy, with basis the beginning and the end points, and restricted by lattice automorphs with a varying value of the trace. Both ways of looking lead to the concept of a *family* of growth boundaries (and of automorphs).

4.1. Families of boundaries. Selection rules

A given family of growth boundaries is fixed by two lattice points $P(a) = [p_1\, p_2]$ and $Q(a) = [q_1\, q_2] \in \Lambda$ representing the end points of the boundary, where $a = \{a_1, a_2\}$ indicates the hexagonal lattice basis with respect to which the integral components p_1, p_2, q_1, q_2 are expressed. Only admitted are pairs of points transformed into another by a lattice automorphism A. The concept of family arises because, if for the given pair P, Q one automorph exists (as it is assumed), there is also an infinite set of them. To begin with the notation for a family F_h (where the subscript refers to hexagonal), one has:

$$F_h: \quad P(a) = [p_1\, p_2] \overset{A}{\rightarrow} Q(a) = [q_1\, q_2] \quad A(a) \in GL(2, \mathbb{Z}). \tag{26}$$

A growth boundary is not oriented: beginning and end points are only distinguished by the automorph A, and are interchanged if one takes A^{-1}.

Let us consider the lattice vector $v = [v_1\, v_2]$ connecting beginning with end: $v = Q(a) - P(a)$. As already discussed in the parabolic case, there is then a reciprocal-lattice vector $k = (k_1\, k_2) \in \Lambda^*$ perpendicular to v:

$$k \cdot v = k_1 v_1 + k_2 v_2 = 0. \tag{27}$$

Without restriction of generality, one can assume that the integral components of k are relatively prime: $(k_1, k_2) = 1$. So a family fixes a reciprocal-lattice vector k, common to all growth boundaries of the family. The converse is not true. First of all, a given k neither fixes the lattice line (its orientation only) nor the pair of beginning–end points on the line. Furthermore, there are pairs of lattice points not connected by any automorph. The automorphs belonging to a given family have a different trace, which takes an integral value n between -2 and ∞. Therefore, in a family one always finds an infinite number of hyperbolic automorphs (for $2 < n < \infty$), but at most one parabolic automorph (if $n = 2$ is a solution) and no more than three elliptic ones (requiring $-2 < n < 2$), giving rise to the corresponding crystallographic admitted growth boundaries of the family, which is a discrete set labeled by n. The asymptotic value $n \rightarrow \infty$ is neither crystallographic nor physical. The largest experimentally observed values are $n \approx 5000$. In the drawings of Figs. 1 to 5, smaller values have also been adopted, because in the asymptotic case it is only the order of magnitude of n that matters.

The automorph A is a discrete transformation, whereas a boundary is continuous and generated by continuous transformations. For the parabolic, hyperbolic and elliptic cases, they are respectively indicated in equations (9), (18), (25). These relations are implicitly implied when a family is indicated as in (26). Few families are morphologically important. In the 12 examples of snow flakes shown in Figs. 1 to 5, only the following five families occur (up to a doubtful central pattern of BH 114.8, included in Table 1) together, of course, with those obtained by conjugation with the hexagonal point group, as indicated in Fig. 6. In these families, the beginning and end points are on hexagonal mirror planes and this ensures that the corresponding 6*mm* symmetric boundaries form close patterns. These families are:

$$\mathbf{1F_h}: \quad [1\,0] \rightarrow [1\,1], \quad k = (1\,0). \tag{28}$$

$$A_n(a) = \begin{pmatrix} 1 & n-2 \\ 1 & n-1 \end{pmatrix}, \quad -2 < n < \infty, \quad \tan\phi_n = 1/3^{1/2};$$

$$\text{hyperbolic}: \quad 2 < n < \infty, \quad \sigma_n = \frac{3^{1/2}(n-2)^{1/2}}{(n+2)^{1/2}},$$

$$\cos\omega_n = \tfrac{1}{2}\frac{n-4}{n-1}, \quad \omega_\infty = \pi/3;$$

$$\text{elliptic}: \quad -2 < n < 2, \quad \rho_n = -\frac{3^{1/2}(2-n)^{1/2}}{(n+2)^{1/2}};$$

$$\text{parabolic}: \quad n = 2, \quad P(e) = \begin{pmatrix} \frac{1}{2} & -1/(2\times 3^{1/2}) \\ 3^{1/2}/2 & \frac{3}{2} \end{pmatrix}.$$

This family is the most important. It is the only one that includes the regular hexagon, obtained for $n = 2$. Therefore, the appearance of a hexagon in the patterns of a snow flake fixes the orientation of the growth lattice (which in this paper is in the x orientation), but not necessarily in the same orientation as the underlying microscopic lattice, which could possibly have the alternative y orientation, as discussed in §2. Hexagonal boundaries allowed by this family are shown in Fig. 6. The regular hyperbolic hexagon (for $n = 4$) characterized by edges intersecting at an angle of 60° instead of the usual 120°, and obtained from an automorph belonging to the point group of the ice crystal, also occurs in the family $2F_h$ with the alternative orientation.

$$\mathbf{2F_h}: \quad [1\,\bar{1}] \rightarrow [2\,1], \quad k = (2\,\bar{1}). \tag{29}$$

$$A_n(a) = \begin{pmatrix} 2m+1 & 2m-1 \\ m+1 & m \end{pmatrix}, \quad n = 3m+1, \quad \tan\phi_n = 0;$$

hyperbolic : $2 < n < \infty$, $\sigma_n = \dfrac{(3m-1)^{1/2}}{(m+1)^{1/2}}$,

$$\cos\omega_n = \tfrac{1}{2}(m-1)/m, \quad \omega_\infty = \pi/3;$$

elliptic : $-2 < n < 2$ $\rho_n = -1$, circle;

parabolic : forbidden.

This family describes hexagonal boundaries in an orientation turned by 90° with respect to the first family but, in the present case, in addition to the general selection rule $-2 < n < \infty$, the possible growth boundaries are restricted by the condition

$$n = 3m+1, \quad m \in \mathbb{N}, \tag{30}$$

where $\mathbb{N}$ denotes the set of natural integers 0, 1, 2, ... The circular boundary (for $n = 1$) is common to $1F_h$ and $2F_2$, whereas the regular hexagon is here forbidden. The validity of this last selection rule can be verified easily. Indeed, in the more than 2000 snow flakes reproduced in the book by Bentley & Humphreys (1931), I could not find any snow crystal with hexagons in the two orientations allowed by the point group $6/mmm$ of ice. This observation was confirmed by looking at the book *Snow Crystals* issued by the Japanese Snow Museum, where many very nice microphotographs of natural snow crystals taken by Y. Furukawa are reproduced (Furukawa & Kobayashi, 1991). The same cannot be said of hyperbolic boundaries. The two alternative orientations can occur in the same snow crystal, as it follows theoretically by considering $1F_h$ and $2F_h$, and as one can see empirically, by looking at Figs. 1 to 5. In the collection of Furukawa's micrographs, one finds a very nice example where the dendritic branches are consistent with both orientations appearing together and give the impression of 12-fold symmetry.

$$\mathbf{3F_h}: \quad [1\,0] \;\rightarrow\; [2\,1], \quad k = (1\,\bar{1}). \tag{31}$$

$$A_n(a) = \begin{pmatrix} 2 & 2n-5 \\ 1 & n-2 \end{pmatrix}, \quad -2 < n < \infty,$$

$$\tan\phi_n = \frac{3^{1/2}(n-3)}{3n-5+2D^{1/2}}, \quad D = 3n^2 - 12n + 13;$$

hyperbolic : $2 < n < \infty$, $\sigma_n = \dfrac{3n-8+2D^{1/2}}{3^{1/2}(n^2-4)^{1/2}}$,

$$\cos\omega_n = \frac{1}{2}\frac{3n-8}{D^{1/2}}, \quad \omega_\infty = \pi/6$$

elliptic : $-2 < n < 2$, $\rho_n = \dfrac{3n-8+2D^{1/2}}{3^{1/2}(4-n^2)^{1/2}}$;

parabolic : $n = 2$, $P(e) = \begin{pmatrix} \frac{3}{2} & -1/2 \times 3^{1/2} \\ 3^{1/2}/2 & \frac{1}{2} \end{pmatrix}$.

The corresponding enantiomorphic family, with expressions obtained by a mirror transformation m, is given by

$$\mathbf{m3F_h}: \quad [1\,0] \;\rightarrow\; [1\,\bar{1}], \quad k = (0\,1). \tag{32}$$

The possible hexagonal boundaries of these two families are shown in Fig. 6. In the snow crystal BH 145.7 of Fig. 2(*a*), the parabolic case ($n = 2$) forms the external boundary, whereas the elliptic boundaries, given by $n = -1$, appear as the central pattern.

$$\mathbf{4F_h}: \quad [1\,0] \;\rightarrow\; [0\,1], \quad k = (1\,1). \tag{33}$$

$$A_n(a) = \begin{pmatrix} 0 & -1 \\ 1 & n \end{pmatrix}, \quad -2 < n < \infty, \quad \tan\phi_n = -1/3^{1/2};$$

hyperbolic : $2 < n < \infty$, $\sigma_n = -\dfrac{3^{1/2}(n+2)^{1/2}}{(n-2)^{1/2}}$,

$$\cos\omega_n = \tfrac{1}{2}\frac{n+4}{n+1}, \quad \omega_\infty = 2\pi/3;$$

elliptic : $-2 < n < 2$, $\rho_n = -\dfrac{3^{1/2}(2+n)^{1/2}}{(2-n)^{1/2}}$;

parabolic : $n = 2$, $P(e) = \begin{pmatrix} -\frac{1}{2} & -3 \times 3^{1/2}/2 \\ 3^{1/2}/2 & \frac{5}{2} \end{pmatrix}$.

$$\mathbf{5F_h}: \quad [1\,\bar{1}] \;\rightarrow\; [1\,2], \quad k = (1\,0). \tag{34}$$

$$A_n(a) = \begin{pmatrix} m & m-1 \\ 2m+1 & 2m-1 \end{pmatrix}, \quad -2 < n < \infty,$$

$$\tan\phi_n = 1/3^{1/2}, \quad n = 3m-1;$$

hyperbolic : $2 < n < \infty$, $\sigma_n = \dfrac{(m-1)^{1/2}}{(3m+1)^{1/2}}$,

$$\cos\omega_n = -\frac{1}{2}\frac{m+1}{m}, \quad \omega_\infty = 2\pi/3;$$

elliptic : $-2 < n < 2$, $\rho_n = -1$ circle;

parabolic : $n = 2$, $P(e) = \begin{pmatrix} -\frac{1}{2} & -3^{1/2}/2 \\ 3 \times 3^{1/2}/2 & \frac{5}{2} \end{pmatrix}$.

These last two families are in an alternative orientation, like the first two families. Again, $5F_h$, in the *y* orientation, implies stronger selection rules than $4F_h$, owing to the additional condition for the trace $n = 2 \bmod 3$. The most interesting type of boundary belonging to these families is the *star hexagon*, obtained for $n = 2$. The possibility of star hexagons in the two alternative orientations is consistent with the two types of hexagrammal scaling relations of the mid-edge and of the vertex type, respectively, discussed in a previous work (Janner, 2001*a*). In snow crystals, one finds many cases with a star hexagon belonging to $5F_h$, and apparently not those oriented as in $4F_h$. Perhaps this fact is related to the absence of hexagons in the *y* orientation, as pointed out above.

4.2. Main and satellite boundaries

All boundaries considered so far are centered at the origin of the overall sixfold point symmetry of the snow crystal. There are other boundaries as well. Typically in dendritic snow crystals, one also finds branching points outside the origin (see for example BH 167.8) and in facet-like crystals one observes off-center regular hexagons (see BH 68.8 and BH 114.8). These observations lead to a distinction between *main*

boundaries and *satellite boundaries*, having their respective centers at a lattice point coinciding, or not, with the origin. The nomenclature has been taken over from crystal diffraction.

Satellite growth boundaries differ from the main ones in two respects:

(i) by a shift of origin of the family of possible boundaries by a vector of the growth lattice;

(ii) by the non-shifted hexagonal symmetry applied to the boundaries of the shifted family.

The samples chosen in Figs. 3 and 4 show that satellite boundaries sometimes have centers at end points of occurring main boundaries (BH 33.5, BH 114.8, BH 167.8), but sometimes the centers are not related to visible morphological features, even if still belonging to the growth lattice (BH 63.12, BH 145.12).

Satellite boundaries seem to be more restricted than the main boundaries. One mainly finds circular, hexagonal and the hyperbolic degenerate ones. Perhaps this is only because it is easier to visualize the corresponding centers in these cases than in the other ones.

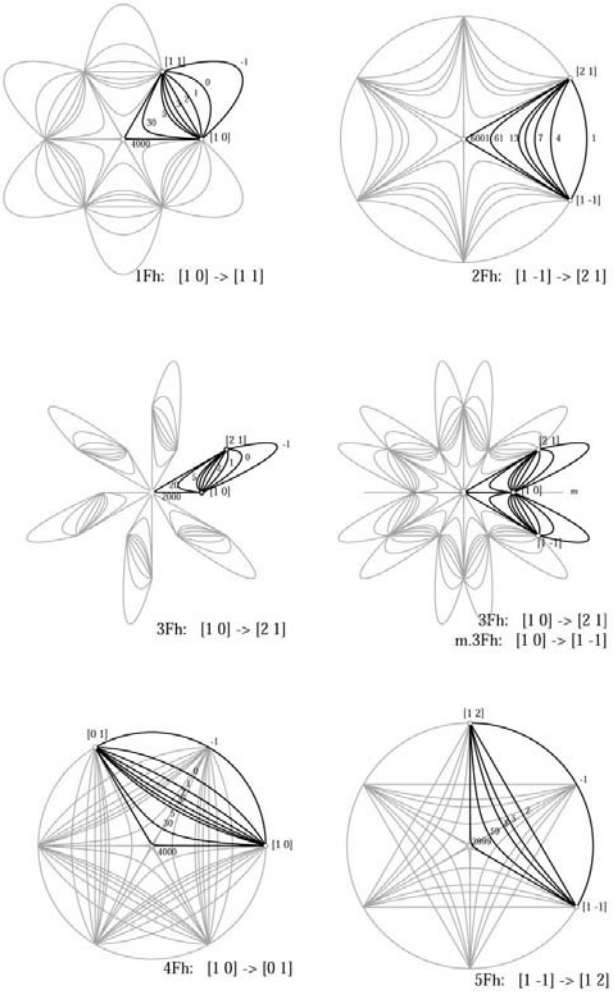

Figure 6
Shown are the most important families of indexed hexagonal growth boundaries. The boundaries belonging to a given family (in bold) share their beginning and end at points of the growth lattice and are labeled by the trace of the lattice automorph transforming this pair of points into one another along the corresponding boundary line. The possible integral values of the trace are restricted by selection rules that reflect crystallographic conditions.

5. Survey

A survey of the growth boundaries of the 12 snow crystals of Figs. 1 to 5, drawn on the corresponding samples according to the present approach, is given in Table 1. Indicated are, for each sample, the family, the indices and other characteristics.

6. Conclusions

The present geometric investigation represents a further step towards a physical understanding of the morphology of snow crystals. Three main results can be summarized as follows:

(i) The existence of a macroscopic hexagonal lattice (the growth lattice) gives rise to pairs of lattice points pinning the ends of observed continuous patterns (the growth boundaries). The lattice points are probably associated with crystallization seeds, and the boundaries are considered to represent crystal surfaces at stationary steps during growth, favoring an accumulation of impurities.

(ii) The discrete and crystallographic character of the growth boundaries is expressed in terms of integral invertible two-dimensional matrices (automorphs of the growth lattice), allowing the boundaries to be labeled according to a set of rational indices.

(iii) Boundaries having a common pair of end points form a family and are restricted by selection rules for their indices. In the case of regular hexagons, only one of the two orientations allowed by the point group $6/mmm$ can occur in a given snow single crystal.

It is, however, not the case that all snow crystals grow according to these rules. Many more irregular snow flakes exist and are observed, in particular in the dendritic case. Possibly, the concentration of the type of impurities giving rise to seeds and responsible for the formation of a growth lattice plays a crucial role. The present analysis, based on more general crystallographic principles than those usually admitted, allows one to recognize a hidden order in what, at first, appears as purely accidental.

APPENDIX *A*

This Appendix indicates how the formula of the hyperbolic and the elliptic cases have been derived. Starting from the automorph

$$A(a) = \begin{pmatrix} n-\delta & \beta \\ [(n-\delta)\delta - 1]/\beta & \delta \end{pmatrix}, \quad n, \beta, \delta \in \mathbb{Z}, \qquad (35)$$

satisfying the conditions given in equation (3), one determines the eigenvectors:

$$v_\pm = \beta a_1 + \left[-\frac{n}{2} \pm \frac{(n^2-4)^{1/2}}{2} + \delta \right] a_2 = x_\pm e_1 + y_\pm e_2. \quad (36)$$

Table 1
Survey of the indexed boundaries of the snow crystals of Figs. 1 to 5; *M* and *S* indicate the main and satellite boundary type, respectively.

Sample	Family	Basis	End points (center)	Unit(s)	Trace	Type	Shape
BW 1	$1F_h$	a	[1 0] – [1 1] ([0 0])	$u = 1$	$n = 2$	*M*	Hexagon
				$u = 2$	$n = 5$	*M*	Hyperbola
BH 105.3	$1F_h$	a	[1 0] – [1 1] ([0 0])	$u = 1, 2, 3$	$n = 2$	*M*	Hexagons
				$u = 8$	$n = 12$	*M*	Hyperbola
BH 109.7	$1F_h$	a	[1 0] – [1 1] ([0 0])	$u = 1, 2, 4, 5, 6$	$n = 2$	*M*	Hexagons
				$u = 12$	$n = 5$	*M*	Hyperbola
					$n = 200$	*M*	Hyperbola
BH 27.3	$1F_h$	a	[1 0] – [1 1] ([0 0])	$u = 2, 3, 4$	$n = 2$	*M*	Hexagons
				$u = 2$	$n = 300$	*M*	Hyperbola
	$2F_h$	a	[1 $\bar{1}$] – [2 1] ([0 0])	$u = 1$	$n = 40$	*M*	Hyperbola
				$u = 2$	$n = 4$	*M*	Hyperbola
BH 145.7	$3F_h$	a	[1 0] – [2 1] ([0 0])	$u = 1$	$n = -1$	*M*	Ellipse
				$u = 6$	$n = 2$	*M*	Straight line
				$u = 6$	$n = 2000$	*M*	Hyperbola
BH 39.8	$1F_h$	$a_0 = a/6$	$[1\ 0]_0$ – $[1\ 1]_0$ ([0 0])	$u_0 = 1$	$n = 1$	*M*	Circle
		a	[1 0] – [1 1] ([0 0])	$u = 1, 4$	$n = 2$	*M*	Hexagons
				$u = 3$	$n = 8$	*M*	Hyperbola
				$u = 4$	$n = 2000$	*M*	Hyperbola
		$a_0 = a/6$	$[1\ 0]_0$ – $[1\ 1]_0$ ($[0\ 2]_0$)	$u_0 = 1$	$n = 1$	*S*	Circle
BH 33.5	$1F_h$	a	[1 0] – [1 1] ([0 0])	$u = 2, 5$	$n = 2$	*M*	Hexagons
	$1F_h$	a	[1 $\bar{1}$] – [2 1] ([2 0])	$u = 1$	$n = 1$	*S*	Circle arc
BH 145.12	$1F_h$	a	[1 0] – [1 1] ([0 0])	$u = 1$	$n = 3, 5$	*M*	Hyperbolas
	$4F_h$	a	[4 0] – [3 1] ([3 0])	$u = 1$	$n = 4000$	*S*	Hyperbola
	$1F_h$	$a_0 = a/3$	$[4\ \bar{4}]_0$ – $[8\ 4]_0$ ($[8\ 0]_0$)	$u_0 = 4$	$n = 1$	*S*	Circle arc
BH 63.12	$1F_h$	a	[1 0] – [1 1] ([0 0])	$u = 1, 3$	$n = 2$	*M*	Hexagons
	$2F_h$	a	[1 $\bar{1}$] – [2 1] ([0 0])	$u = 1$	$n = 1$	*M*	Circle
	$1F_h$	$a_1 = 3a$	$[1\ \bar{1}]_1$ – $[2\ 1]_1$ ($[2\ 0]_1$)	$u_1 = 1$	$n = 1$	*S*	Circle arc
BH 68.8	$1F_h$	$a_0 = a/3$	$[1\ 0]_0$ – $[1\ 1]_0$ ([0 0])	$u_0 = 1, 3$	$n = 2$	*M*	Hexagons
	$5F_h$	a	[1 $\bar{1}$] – [1 2] ([0 0])	$u = 1$	$n = 2$	*M*	Star hexagon
	$2F_h$	a	[2 $\bar{1}$] – [3 1] ([1 0])	$u = 1$	$n = 2000$	*S*	Hyperbola
	$4F_h$	a	[3 1] – [1 3] ([1 1])	$u = 1$	$n = 2000$	*S*	Hyperbola
BH 114.8	$1F_h$	$a_0 = a/2$	$[1\ 0]_0$ – $[1\ 1]_0$ ([0 0])	$u_0 = 1$	$n = 2$	*M*	Hexagon
		a	[1 0] – [1 1] ([0 0])	$u = 1, 2$	$n = 2$	*M*	Hexagons
	$5F_h$	a	[1 $\bar{1}$] – [1 2] ([0 0])	$u = 1$	$n = 2$	*M*	Star hexagon
	–	$a_0 = a/9$	$[3\ \bar{2}]_0$ – $[3\ 1]_0$ ([0 0])	$u_0 = 1$	$n = 1,7$	*M*	Circle-hyperbola
	$2F_h$	a	[2 $\bar{1}$] – [3 1] ([1 0])	$u = 1$	$n = 2000$	*S*	Hyperbola
	$4F_h$	a	[3 1] – [1 3] ([1 1])	$u = 1$	$n = 2000$	*S*	Hyperbola
BH 167.8	$1F_h$	a	[1 0] – [1 1] ([0 0])	$u = 1, 2, 3$	$n = 2$	*M*	Hexagons
	$2F_h$	$a_0 = a/2$	$[1\ \bar{1}]_0$ – $[2\ 1]_0$ ([0 0])	$u_0 = 1$	$n = 6001$	*M*	Hyperbola
	$4F_h$	$a_1 = 3a$	$[2\ 1]_1$ – $[1\ 2]_1$ ($[1\ 1]_1$)	$u_1 = 1$	$n = 2000$	*S*	Hyperbola
		$a_1 = 3a$	$[3\ 2]_1$ – $[2\ 3]_1$ ($[2\ 2]_1$)	$u_1 = 1$	$n = 2000$	*S*	Hyperbola

The corresponding eigenvalues are:

$$\lambda_{\pm} = \frac{n}{2} \pm \frac{(n^2-4)^{1/2}}{2}. \tag{37}$$

The orientation of the rotated orthonormal basis e' is given by

$$\tan\phi_n = \frac{x_+y_- + x_-y_+}{x_+x_- - y_+y_- + r_+r_-} = \frac{z_2}{z_3 + r_{12}}, \tag{38}$$

with

$$\phi_n = (\phi_+ + \phi_-)/2, \quad \tan\phi_\pm = y_\pm/x_\pm,$$
$$r_\pm = (x_\pm^2 + y_\pm^2)^{1/2}, \quad r_{12} = r_+r_- \tag{39}$$

and z_0, z_1, z_2, z_3 are as in equation (17). From the scalar product $v_+ \cdot v_-/r_+r_-$, one derives the angle ω_n between the eigenvectors.

For $n^2 > 4$, one finds:

$$\frac{x_+x_- + y_+y_-}{r_+r_-} = \frac{(\beta/2-\delta)n + z_0 + 1}{r_+r_-} = \frac{z_1}{r_{12}} = \cos\omega_n. \tag{40}$$

This angle is related to the affine deformation factor σ_n by

$$\sigma_n = \frac{1+\cos\omega_n}{\sin\omega_n} = \left(\frac{r_{12}+z_1}{r_{12}-z_1}\right)^{1/2}, \tag{41}$$

which, by using the relation $(r_{12}^2 - z_1^2)^{1/2} = (3^{1/2}/2)\beta(n^2-4)^{1/2}$, becomes equivalent to equation (14).

Correspondingly, for $n^2 < 4$, one has $x_+x_- + y_+y_- \geq r_+r_-$, implying $z_1 \geq r_{12}$, so that

$$(z_1^2 - r_{12}^2)^{1/2} = (3^{1/2}/2)\beta(4-n^2)^{1/2}, \tag{42}$$

leading to the affine deformation factor for the elliptic case:

$$\rho_n = \frac{2}{3^{1/2}}\frac{z_1 + r_{12}}{\beta(4-n^2)^{1/2}} = \left(\frac{z_1+r_{12}}{z_1-r_{12}}\right)^{1/2}. \tag{43}$$

In particular, the circular case is characterized by the relations

$$\rho_n^2 = 1 \Longleftrightarrow r_{12} = -r_{12} = 0. \tag{44}$$

Thanks are expressed to B. Souvignier for valuable remarks and suggestions and to Annalisa Fasolino for stimulating discussions.

References

Bentley, W. A. & Humphreys, W. J. (1931). *Snow Crystals*. New York: McGraw-Hill. Reprinted by Dover 1962.
Furukawa, Y. & Kobayashi, T. (1991). *Snow Crystals*. Japanese Snow Museum, Asahikawa, Hokkaido. (Japanese edition.)
Janner, A. (1996). *Acta Cryst.* A**52**, C-549.
Janner, A. (1997). *Acta Cryst.* A**53**, 615–631.
Janner, A. (2001*a*). *Cryst. Eng.* **4**, 119–129. Special issue for the Indaba III Conference.
Janner, A. (2001*b*). *Acta Cryst.* A**57**, 378–388.
Olovsson, I. (1985). *Bild Wiss.* **12**, 50–59.